Applied Physics Letters ARTICLE scitation.org/journal/apl

Light-emitting diodes with AlN polarization-induced buried tunnel junctions: A second look

Cite as: Appl. Phys. Lett. **117**, 061104 (2020); doi: 10.1063/5.0015097
Submitted: 24 May 2020 · Accepted: 28 July 2020 ·
Published Online: 11 August 2020

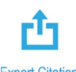

Kevin Lee,[1,a)] Shyam Bharadwaj,[1] Yu-Tsun Shao,[2] Len van Deurzen,[2] Vladimir Protasenko,[1] David A. Muller,[2,3] Huili Grace Xing,[1,3,4] and Debdeep Jena[1,3,4]

AFFILIATIONS

[1]School of Electrical and Computer Engineering, Cornell University, Ithaca, New York 14853, USA
[2]Applied and Engineering Physics, Cornell University, Ithaca, New York 14853, USA
[3]Kavli Institute at Cornell for Nanoscale Science, Cornell University, Ithaca, New York 14853, USA
[4]Department of Materials Science and Engineering, Cornell University, Ithaca, New York 14853, USA

[a)]Author to whom correspondence should be addressed: kl833@cornell.edu

ABSTRACT

Interband Zener tunneling of electrons has been recently used in III-nitride semiconductor based light emitters to efficiently inject holes into p-cladding layers. Zener tunneling probabilities can be significantly enhanced if crystal symmetry-induced internal polarization fields assist the dopant-induced built-in electric fields of tunnel junctions because of the large reduction of the tunneling distance. In a metal-polar buried tunnel junction geometry, such electric field alignment needs an AlN interlayer at the tunnel junction. Because AlN is a larger bandgap semiconductor than GaN, it is not clear *a priori* if the net tunneling probability is reduced or enhanced compared to a homojunction. By combining theoretical modeling with experimental blue light emitting diodes, we find that the large tunneling enhancement due to the polarization field and band realignment overcome the reduction in tunneling due to the larger bandgap of AlN. Compared to a homojunction tunnel-junction, the inclusion of AlN in the tunnel junction is found to lower the turn-on and operating voltages and increase the wall-plug efficiency. This proves that polarization-induced AlN tunnel junctions are superior to homojunctions at low injection currents, resulting in higher optical emission intensity and superior uniformity.

Published under license by AIP Publishing. https://doi.org/10.1063/5.0015097

Tunnel-junction (TJ) light-emitting diodes (LEDs) based on III-nitride semiconductors have been extensively investigated in the past few years by various growth techniques including metal-organic chemical vapor deposition (MOCVD), molecular beam epitaxy (MBE), and hybrid MOCVD + MBE.[1–6] TJ LEDs utilize interband tunneling to inject holes into the active region. It eliminates the need for Ohmic contacts to p-GaN; the contacts instead made to n-GaN layers result in ~3 orders lower resistivity and efficient current spreading.[7,8] The majority of the efforts have employed top tunnel junction (TTJ) geometry, in which the TJ is placed on top of the p-layer, which is above the multiple quantum well active region in a p-up geometry.[9,10]

Recently, a new strategy was demonstrated using bottom or buried homojunction TJs (BTJs).[11–13] In contrast to TTJ LEDs, the TJ in BTJ LEDs is underneath the active region in a p-down geometry. The flipped structure realizes the favorable N-polar-like orientation of the electric fields inside the active region in a Ga-polar structure, providing superior hole confinement and suppressing cladding layer emission from carrier overflow.[14]

In both TTJ and BTJ structures, the interband tunneling probability of electrons is estimated from the Wentzel–Kramers–Brillouin (WKB) approximation by $T_{WKB} \sim \exp(-2\int_0^{w_d} k(x)dx)$, where $k(x) = \sqrt{2m^*\mathcal{V}(x)}/\hbar$.[15] Here, w_d is the depletion width of the TJ and $\mathcal{V}(x)$ is the potential barrier profile through which electrons must tunnel, m^* is the reduced tunneling effective mass, and $\hbar$ is the reduced Planck constant. The depletion width is dependent on the doping concentrations of both the n-type and p-type sides. Increasing the doping shrinks the depletion width, increasing the tunneling probability. Okumura *et al.* calculated tunneling probabilities for GaN homojunctions of a fixed doping Si donor concentration of 10^{20} cm^{-3} for various Mg doping concentrations. Increasing Mg doping from 3×10^{19} cm^{-3} to 10^{20} cm^{-3} has the potential to increase the tunneling probability by ~17 orders of magnitude. However, the high doping of Mg in GaN

results in crystal degradation and self-compensation, reducing the free hole carrier concentration.[16,17] As a result, the TJ depletion width increases and tunneling probability falls, making homojunction TJs resistive. Midgap defects can enable tunneling currents, but to boost the junction electric field without intentionally introducing defects, one can turn to the internal polarization fields of nitride semiconductor heterojunctions along the polar $\pm c$-axis direction.

In the metal polar $+c$-axis direction, aligning the polarization field in a heterojunction with the built-in dopant-induced field of the p–n TJ enhances the tunneling probability.[18] Achieving this alignment requires different geometries for TTJ and BTJ.[19] For the TTJ geometry, the built-in field of the TJ points along the -c-axis. Inserting InGaN in the TJ will create a spontaneous polarization field along the -c-axis for In < 80% or the $+c$-axis for In > 80%. The piezoelectric polarization field created by InGaN will be along the -c-axis.[20] The resulting net polarization field points in the -c-axis, which is aligned with the built-in junction field.[1,3] This study focuses on structures using metal-polar n-type GaN substrates that are the most common for blue LEDs. For the BTJ geometry, the built-in junction field is along the $+c$-axis direction, from the n-type substrate to the buried p-layer. Instead of InGaN, it is, then, necessary to use AlGaN for the correct alignment of the polarization field since both the spontaneous and piezo-polarization fields point in the $+c$-axis direction.[21] Using a BTJ geometry with an AlN interlayer prevents reabsorption of the photons emitted from the active regions, which could occur in InGaN TJs, for which enhancing the tunneling probability requires the use of high indium-content (In > 15%) layers.[22] If the active region also consists of InGaN multiple quantum wells (MQWs), the InGaN TJ partially absorbs the blue emission directed toward the surface. This absorption can be avoided by using wider-gap Al(Ga)N BTJ geometry.

TJs with AlN interlayers have been studied both theoretically and experimentally in the past by several groups. Grundmann and Mishra were the first to experimentally demonstrate the use of AlN TJs in cascaded LED structures to achieve multiple emission wavelengths from a single device.[18] Simon *et al.* studied the transport physics of polarization-induced tunneling junctions and found that there exists a critical thickness to achieve effective type-III broken gap band alignment, which is most desirable for tunneling.[23] This critical thickness is $t_{critical} = E_{g,GaN}/qF_{\pi,GaN/AlN} \sim 2.8\,\text{nm}$, where $E_{g,GaN} = 3.4\,\text{eV}$ is the bandgap of GaN, q is the electron charge, and $F_{\pi,GaN/AlN}$ is the polarization field created in the heterojunction between GaN and AlN. Further increasing the AlN interlayer thickness decreases the tunneling probability. By studying such junctions with band mixing using a 8×8 k·p model, Schubert *et al.* suggested that increasing the AlN insertion thickness to ∼3.5 nm decreases the tunneling current under reverse bias.[24] Kuo *et al.* compared cascaded LEDs with two TJ designs of n++GaN/p++$In_{0.1}Ga_{0.9}N$ and n++GaN/i-AlN/i-GaN/i-AlN/p++GaN with a standard p-up LED.[25] The result shows 80% improvement of light output power from n++GaN/i-AlN/i-GaN/i-AlN/p++GaN TJ-LEDs over standard p-up LEDs.

Thus, though previous studies have demonstrated the successful use of polarization-induced AlN TJs in LEDs, the structures studied have either multiple active regions or TJ designs from which it is difficult to isolate the effect of the TJ itself on the device performance. This motivates a second look at the problem. To identify the role of the AlN polarization-induced TJ, in this work, we compare two simplified LED structures with buried TJs, which are nominally identical in layer thicknesses, doping, and active region. The only difference between them is the insertion of a thin AlN interlayer in one. This simplification enables us to identify the similarities and highlights the differences between a homojunction TJ and a polarization induced AlN interlayer TJ for BTJ LEDs.

The energy band diagrams of the TJs alone studied in this work are shown in Fig. 1(a) for a homojunction TJ and in Fig. 1(b) for an AlN TJ at a reverse bias of -0.5 V as calculated by SiLENSe. When an electron in the valence band in the p-side tunnels through the barrier, it leaves behind a hole that travels in the opposite direction—toward the LED active region on the left. This is hole injection by tunneling. Comparison of Figs. 1(b) and 1(a) shows that inserting an AlN layer at the junction dramatically reduces the depletion width. The band diagram for the homojunction TJ in Fig. 1(a) assumes a reverse bias of -0.5 V near the onset of tunneling, and experimental doping profiles of Mg and Si are discussed later. A piece-wise WKB technique is used to calculate the tunneling probability spectra resolved in energy.[26] The tunneling probability for an ideal GaN homojunction at -0.5 V is $\sim 10^{-38}$, extremely low, yet expected due to the wide bandgap of GaN in the absence of trap-assisted processes. Figure 1(b) shows that the enormous polarization field due to the AlN interlayer greatly reduces the depletion width from ∼20 nm down to ∼3 nm (the AlN barrier thickness) and further creates an accumulation region, boosting the tunneling probability by ∼29 orders of magnitude to 10^{-9}. It is further seen that at extremely high reverse bias voltages, the enhancement of the AlN TJ tunneling probability is nominal, but a larger tunneling window of energies become available. A large reverse bias also causes a giant enhancement of the tunneling probability of the homojunction

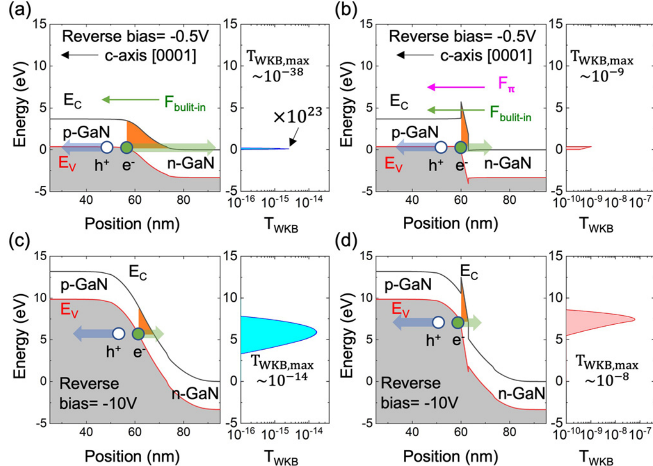

FIG. 1. Energy band diagrams for (a) a homojunction GaN tunnel junction and (b) an AlN polarization-induced tunnel junction at a reverse bias of -0.5 V. The orange shaded area is the barrier through which electrons must tunnel. The plots on the right of the energy band diagrams show the energy-resolved tunneling probability. Si and Mg doping concentrations are set according to the experiment. $F_{built-in}$ is the electric field created by dopants in the p-n junction, and F_π is the field due to polarization charges at the hetero-interfaces. The energy band diagrams under a reverse bias of -10 V for the (c) homojunction GaN tunnel junction and (d) the AlN polarization-induced TJ. Note the extreme advantage of the AlN TJ vs the GaN TJ at low biases, which persists to high bias voltages as indicated by the tunneling probabilities.

Published under license by AIP Publishing

TJ. Thus, the theoretical model predicts that at low reverse bias voltages, the AlN TJ to be far more efficient in hole injection than the homojunction TJ. The difference should reduce for large reverse biases. This prediction from the model was, then, put to test in the experiment.

Figure 2(a) shows the LED layer structures with InGaN multiple quantum well active regions, in which the BTJ structures were experimentally implemented. Plasma-assisted molecular beam epitaxy (PA-MBE) was used to grow the layer structures on Ga-polar n-type GaN substrates. The low background hydrogen level in the MBE environment eliminates the need of post-growth annealing to activate Mg-doped GaN.[27] This "conductive as-grown" property of the p-type layer is crucial for BTJ LEDs that have the p-down geometry, which aligns of the internal polarization fields in the InGaN MQW active regions along the built-in field, in addition to the correct alignment in the AlN-interlayer BTJ.

Two samples were grown: a BTJ LED with a homojunction TJ and a BTJ LED with an $\sim$3 nm AlN interlayer in the TJ as shown in Fig. 2(a). Both were grown on *c*-plane single crystal Ge-doped n-type GaN substrates with a dislocation density in the range of $\sim 5 \times 10^5$ to 3×10^6 cm^{-2}. The growths were performed using a Veeco Gen10 MBE system. The plasma power during growth was 400 W at 2 sccm N_2 flow corresponding to a growth rate of 450 nm/h. During the growth, reflection high energy electron diffraction (RHEED) was employed to monitor the surface and maintain a slightly metal-rich

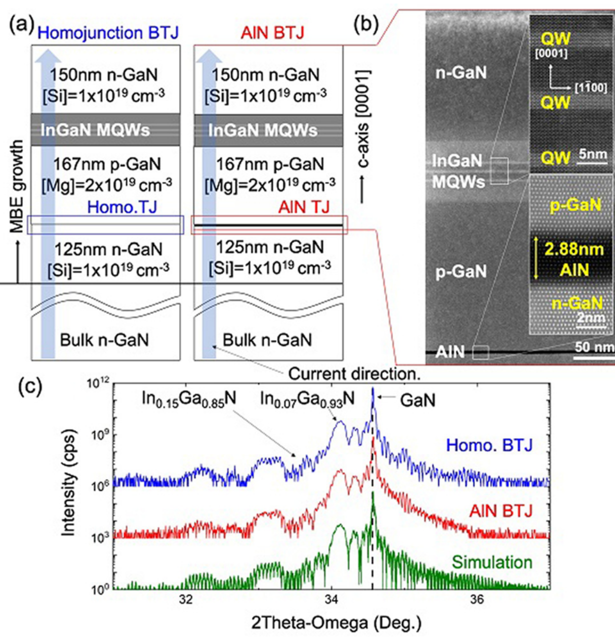

FIG. 2. (a) Epitaxial layer structures for the homojunction BTJ and the AlN BTJ LEDs. Gray layers correspond to the InGaN MQW active region. (b) HAADF-STEM image shows the cross section of the AlN BTJ LED along the a-plane. Top and bottom insets are enlarged images of the multiple InGaN quantum wells and the AlN tunnel junction, respectively. (c) High resolution x-ray 2θ-ω scans along the (002) direction for homojunction BTJ (top), AlN BTJ (middle), and simulated curve (bottom) using the parameters shown in the layer structures. The peaks other than the major labeled ones of GaN, $In_{0.07}Ga_{0.93}N$, and $In_{0.15}Ga_{0.93}N$ and the fringes are

condition to promote 2D growth.[28] All n-type Si-doped GaN layers were grown at a thermocouple temperature of 760 °C with a silicon doping concentration [Si] $= 10^{19}$ cm^{-3}. The Mg-doped GaN layers had a doping concentration [Mg] $= 2 \times 10^{19}$ cm^{-3}. Because Mg incorporation is dependent on growth temperature,[29] a Ga metal desorption test was performed prior to the p-GaN growth to confirm consistency in the surface temperature between the two samples.[30] After the p-GaN layer, the growth was paused to allow excess Ga on the surface to desorb, following which the substrate temperature was reduced to 660 °C to grow the InGaN MQWs and cladding layers. After the active region growth, the substrate temperature was raised back to 760 °C to grow the final 150 nm n-GaN layer. For the BTJ LED with the AlN polarization engineered interlayer, an interrupt was introduced after the initial n-GaN, and migration enhanced epitaxy[31] was used to grow the AlN layer: first, Al was deposited at 760 °C for 28 s, followed by exposure to nitrogen plasma to form the AlN layer. The Al flux and deposition time were calibrated with a separate sample to result in $\sim$3 nm AlN. This process is monitored by RHEED to ensure that no residual Al remains on the surface that could interfere with the subsequent p-GaN growth. Gallium droplets observed after growth were removed by HCl.

The atomic force microscopy image (not shown) revealed atomic steps on both samples with sub-nm roughness over a $2 \times 2\,\mu$m^2 area. To examine the buried AlN thickness and the active regions, scanning transmission electron microscopy (STEM) was performed. Focused ion beam (FIB) was used to lift-out and mill a cross sectional specimen from the AlN BTJ sample. Figure 2(b) shows a STEM image using the high-angle annular-dark-field (HAADF) mode of the cross section of AlN BTJ LEDs. The MQWs and $\sim$2.9 nm AlN are grown uniformly across the field of view, and the three InGaN quantum wells in the active region are clearly resolved. In addition, no dislocations were observed over the 15 μm wide specimen. A high-resolution x-ray 2θ-ω scan (performed using a Panalytical X'pert with a triple-axis detector) along the (002) direction is shown in Fig. 2(c). Fitting the spectra to a simulation shows that the MQWs consist of a 22 nm $In_{0.07}Ga_{0.93}N$ bottom cladding, three periods of 2.8 nm $In_{0.15}Ga_{0.85}N$/7 nm $In_{0.07}Ga_{0.93}N$, and an 18 nm $In_{0.07}Ga_{0.93}N$ top cladding, which is identical for both BTJ samples, with and without the AlN interlayer. The very thin AlN interlayer is not visible in x-ray diffraction.

The two samples were processed into LEDs by performing mesa isolation with inductively coupled plasma reactive etching (ICP-RIE), resulting in an etch depth of $\sim$530 nm, followed by 25/100 nm Ti/Al metallization for both top and bottom n-type contacts. Transmission line measurements revealed a contact resistance of $\sim 6.2 \times 10^{-5}$ for the homojunction BTJ and $\sim 7.76 \times 10^{-6}$ $\Omega\cdot$cm^2 for the AlN BTJ. Figure 3(a) shows the measured I–V characteristics on 80×80 μm^2 devices. The 80×80 μm^2 devices are chosen as representative for I–V because luminescence is uniform for this device size, suggesting uniform current spreading as shown in the inset images of Fig. 4(a). The homojunction BTJ shows a turn-on around -4 V and reaches 50 A/cm^2 at -8.3 V. The AlN BTJ turns on at -2.7 V and reaches 50 A/cm^2 at -6.45 V. At a large bias of -9 V, the AlN BTJ LED has twice the current density as the homojunction BTJ LED. These observations of current transport are qualitatively in line with the expectations from the energy band diagram simulations shown in Figs. 1(a) and 1(b).

On-wafer optical measurements were performed by collecting light from the surface of the LEDs. Both the BTJ LEDs show the

Published under license by AIP Publishing

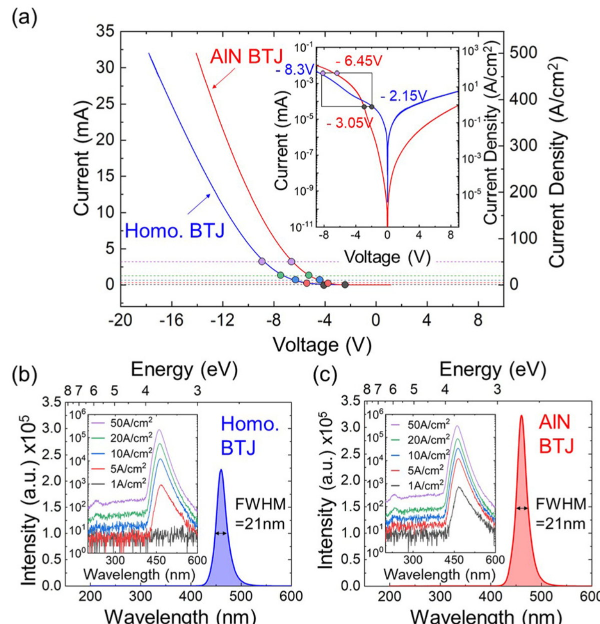

FIG. 3. (a) Current–voltage (I–V) characteristics (left axis) and J–V characteristics (right axis) for the two devices up to 500 A/cm^2. The inset shows a log scale IV curve, indicating a negative voltage turn-on, and the box indicates the region in which electroluminescence was collected. Electroluminescence spectra in the linear scale for (b) the homojunction and (c) the AlN BTJ LED at an injection current density of 50 A/cm^2. Insets show EL spectra on a log scale at various injection current densities. The color of the dots in the IV-curve corresponds to the current density in the inset figures of the EL measurements. Both devices show peak emission at 460 nm, but the AlN BTJ LED has much higher emission at low current densities.

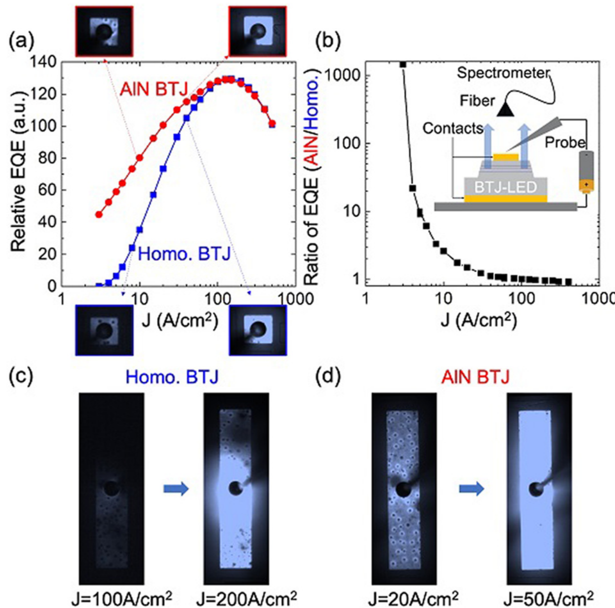

FIG. 4. (a) Relative external quantum efficiencies (EQEs) for the homojunction BTJ vs the AlN polar heterojunction BTJ. The blue curve corresponds to the homojunction BTJ LED and the red curve the AlN polar heterojunction BTJ. The false color images show the LED emission as seen under an optical microscope for a device area of 80×80 μm^2. (b) Ratio of EQE of the AlN BTJ to that of the homojunction BTJ, highlighting a significant advantage of the polar AlN BTJ LED at low injection currents. This advantage persists up to current densities of 100 A/cm^2. The inset figure shows the on-wafer measurement setup. (c) and (d) Larger devices with an area of 100×500 μm^2 operating at different injection current levels. The AlN BTJ LEDs show significantly brighter and uniform emission profiles than the homojunction BTJ LEDs.

primary electroluminescence (EL) peak at 460 nm (2.69 eV) as seen in Figs. 3(b) and 3(c). The linewidth of the emission peak is 21 nm (123 meV) for both the homojunction and AlN BTJ at an injection current density of 50 A/cm^2, indicating similar active regions. Since the EL measurement is performed at a fixed spatial position relative to the detector for both LEDs, approximating the integrated emission intensity to be proportional to the external quantum efficiency (EQE) enables a comparison of the two LEDs at various injection current densities. Figure 4(a) shows the relative EQE for the two samples. The peak EQE for both samples shows similar emission intensity at similar injection current, confirming further that the active regions of the two samples are nearly identical. At the peak EQE injection current of 100 A/cm^2, the differential resistance of the AlN BTJ is $\sim$0.0232 Ω·cm^2, while for the homojunction BTJ, it is 0.0262 Ω·cm^2. Figures 4(c) and 4(d) illustrate the optical emission profile of larger 100×500 μm^2 devices. It can be seen that at a low injection current, the AlN BTJ sample is brighter, and the emission uniformity is superior to the homojunction sample. The difference in the optical recombination efficiency is likely due to the difference in the injected hole/electron ratio at fixed current rather than the difference in the active region since the active regions are similar as per x-ray measurements, the EL peak position, and the linewidth.

Hole injection is a limiting factor in nitride light emitters. For low current densities $<$ 100 A/cm^2, the AlN BTJ LED is observed to have a stronger emission intensity than the homojunction BTJ LED, with a large enhancement at the lowest current levels. This is consistent with the prediction of Figs. 1(a) and 1(b) because at low voltages, the reverse bias in the TJ is low, and the AlN BTJ should inject holes into the LED active region far more efficiently than the homojunction TJ. The EQE is indeed measured to be as much as 100× higher for the AlN polarization-induced BTJ LED at the lowest injected currents than the homojunction BTJ LED, shown in Fig. 4(b). This benefit diminishes at high injection currents, after which both TJs inject a large number of holes, which is also consistent with the expectations outlined from the analysis in Figs. 1(c) and 1(d) vs 1(a) and 1(b). At high reverse-bias voltages, the tunneling probabilities approach similar values, making hole injection into the active region of similar efficiency. The ratio of EQE between the two samples decreases as the injection current increases in proportion to voltage, consistent with this picture. For devices with a larger area of 100×500 μm^2, the significantly increased emission uniformity for the AlN BTJ LED in Fig. 4(d) is explained by the same argument. The homojunction BTJ LED has lower hole current for current densities $<$100 A/cm^2, making its EQE is lower than that of the AlN BTJ LED. To attain the same level of hole current at the BTJ LED, the homojunction BTJ LED requires higher injected current. However, when the total injection current is high, current crowding occurs below the top metal pad, decreasing the current spreading length and resulting in emission mostly near the metal pad and high non-uniformity, as seen vividly in Fig. 4(c).[32]

Published under license by AIP Publishing

The dark spots seen in the AlN BTJ LED at a low current injection of 20 A/cm^2 in Fig. 4(d) are commensurate with a dislocation density of $\sim 10^6$ cm^{-2} of the substrate; they are also seen in the homojunction BTJ LED. Following earlier work of Xu *et al.*,[33] hot phosphoric acid was used to etch the surface. Subsequent AFM mapping showed that some dark spots regions transformed into pits of hexagonal shape upon etching, proving that they are dislocation-related defects. No correlation was found between the dark spot density with device performance, and the spots are not observable at high current injection. The influence and origin of the dark spots will be discussed in a separate work.

In summary, it is found that in comparison to homojunction TJs, the use of polarization engineered AlN interlayers in BTJ blue LEDs increases the efficiency of hole injection at low injection current levels and reduces the turn on voltage. At the same injection current levels, the AlN BTJ LEDs exhibit more uniform emission. The ratio of EQE between the devices reveals that the advantage of the AlN BTJ is the greatest in the low injection current region, at which the difference in hole injection efficiency is maximum. To reach similar current levels, the homojunction BTJ requires higher forward bias voltage. At the peak EQE current density of $\sim$100 A/cm^2, the homojunction BTJ requires $\sim$3 V more driving voltage than the AlN BTJ. Therefore, the AlN BTJ has better wall-plug efficiency than the homojunction device, even at high current levels at which the differences in hole injection become negligible. The results of this work provide an alternative method for reducing TJ resistance and improving the wall plug efficiency for BTJ LEDs, while also aligning the active region's internal polarization field to the built-in dopant-induced p–n junction field. The counterintuitive enhancement of the tunneling current in the BTJ LED geometry in spite of a larger bandgap AlN interlayer is facilitated primarily by the large polarization fields. The comparative study presented here helped identify the regimes in which the advantage could be exploited.

The authors at Cornell University acknowledge the financial support from the Cornell Center for Materials Research with funding from the NSF MRSEC program (No. DMR-1719875) and AFOSR Hybrid Materials MURI under Award No. FA9550-18-1-0480. Device fabrication is performed in part at the Cornell NanoScale Facility, a member of the National Nanotechnology Coordinated Infrastructure (NNCI), which is supported by the National Science Foundation (Grant No. NNCI-1542081). We also acknowledge the electron microscopy facility from the National Science Foundation (Nos. DMR-1719875 and DMR-1429155).

DATA AVAILABILITY

The data that support the findings of this study are available from the corresponding author upon reasonable request.

REFERENCES

[1] S. Krishnamoorthy, F. Akyol, and S. Rajan, Appl. Phys. Lett. **105**, 141104 (2014).
[2] S. M. Sadaf, Y. H. Ra, H. P. T. Nguyen, M. Djavid, and Z. Mi, Nano Lett. **15**, 6696 (2015).
[3] Y. Zhang, S. Krishnamoorthy, J. M. Johnson, F. Akyol, A. Allerman, M. W. Moseley, A. Armstrong, J. Hwang, and S. Rajan, Appl. Phys. Lett. **106**, 141103 (2015).
[4] D. Hwang, A. J. Mughal, M. S. Wong, A. I. Alhassan, S. Nakamura, and S. P. Denbaars, Appl. Phys. Express **11**, 012102 (2018).
[5] E. C. Young, B. P. Yonkee, F. Wu, S. H. Oh, S. P. DenBaars, S. Nakamura, and J. S. Speck, Appl. Phys. Express **9**, 022102 (2016).
[6] Y. Akatsuka, S. Iwayama, T. Takeuchi, S. Kamiyama, M. Iwaya, and I. Akasaki, Appl. Phys. Express **12**, 025502 (2019).
[7] F. Afroz Faria, J. Guo, P. Zhao, G. Li, P. Kumar Kandaswamy, M. Wistey, H. Xing, and D. Jena, Appl. Phys. Lett. **101**, 032109 (2012).
[8] A. Bhattacharyya, W. Li, J. Cabalu, T. D. Moustakas, D. J. Smith, and R. L. Hervig, Appl. Phys. Lett. **85**, 4956 (2004).
[9] M. Malinverni, D. Martin, and N. Grandjean, Appl. Phys. Lett. **107**, 051107 (2015).
[10] C. Skierbiszewski, G. Muziol, K. Nowakowski-Szkudlarek, H. Turski, M. Siekacz, A. Feduniewicz-Zmuda, A. Nowakowska-Szkudlarek, M. Sawicka, and P. Perlin, Appl. Phys. Express **11**, 034103 (2018).
[11] H. Turski, S. Bharadwaj, H. Xing, and D. Jena, J. Appl. Phys. **125**, 203104 (2019).
[12] Y. Cho, S. Bharadwaj, Z. Hu, K. Nomoto, U. Jahn, H. G. Xing, and D. Jena, Jpn. J. Appl. Phys., Part 1 **58**, 060914 (2019).
[13] H. Turski, S. Bharadwaj, M. Siekacz, G. Muziol, M. Chlipala, M. Zak, M. Hajdel, K. Nowakowski-Szkudlarek, S. Stanczyk, H. Xing, D. Jena, and C. Skierbiszewski, "Monolithically p-down nitride laser diodes and LEDs obtained by MBE using buried tunnel junction design," Proc. SPIE Gallium Nitride Materials and Devices XV **11280**, 1128010 (2020).
[14] S. Bharadwaj, J. Miller, K. Lee, J. Lederman, M. Siekacz, H. (Grace) Xing, D. Jena, C. Skierbiszewski, and H. Turski, Opt. Express **28**, 4489 (2020).
[15] S. M. Sze and K. K. Ng, *Physics of Semiconductor Devices* (John Wiley & Sons, Inc., Hoboken, NJ, USA, 2006).
[16] U. Kaufmann, P. Schlotter, H. Obloh, K. Köhler, and M. Maier, Phys. Rev. B **62**, 10867 (2000).
[17] P. Kozodoy, H. Xing, S. P. DenBaars, U. K. Mishra, A. Saxler, R. Perrin, S. Elhamri, and W. C. Mitchel, J. Appl. Phys. **87**, 1832 (2000).
[18] M. J. Grundmann and U. K. Mishra, Phys. Status Solidi C **4**, 2830 (2007).
[19] D. Jena, J. Simon, A. Wang, Y. Cao, K. Goodman, J. Verma, S. Ganguly, G. Li, K. Karda, V. Protasenko, C. Lian, T. Kosel, P. Fay, and H. Xing, Phys. Status Solidi A **208**, 1511 (2011).
[20] C. Wood and D. Jena, *Polarization Effects in Semiconductors: From Ab Initio Theory to Device Applications* (Springer US, Boston, MA, 2008).
[21] L. Li, Y. Zhang, S. Xu, W. Bi, Z. H. Zhang, and H. C. Kuo, Materials **10**, 1221 (2017).
[22] X. Yan, W. Li, S. M. Islam, K. Pourang, H. G. Xing, P. Fay, and D. Jena, Appl. Phys. Lett. **107**, 163504 (2015).
[23] J. Simon, Z. Zhang, K. Goodman, H. Xing, T. Kosel, P. Fay, and D. Jena, Phys. Rev. Lett. **103**, 026801 (2009).
[24] M. F. Schubert, Phys. Rev. B **81**, 035303 (2010).
[25] Y.-K. Kuo, Y.-H. Shih, J.-Y. Chang, W.-C. Lai, H. Liu, F.-M. Chen, M.-L. Lee, and J.-K. Sheu, Opt. Express **25**, A777 (2017).
[26] G. P. Gilfoyle, Comput. Phys. Commun. **121–122**, 573 (1999).
[27] Y. Kuwano, M. Kaga, T. Morita, K. Yamashita, K. Yagi, M. Iwaya, T. Takeuchi, S. Kamiyama, and I. Akasaki, Jpn. J. Appl. Phys., Part 1 **52**, 08JK12 (2013).
[28] B. Heying, R. Averbeck, L. F. Chen, E. Haus, H. Riechert, and J. S. Speck, J. Appl. Phys. **88**, 1855 (2000).
[29] S. Guha, N. A. Bojarczuk, and F. Cardone, Appl. Phys. Lett. **71**, 1685 (1997).
[30] P. Misra, C. Boney, D. Starikov, and A. Bensaoula, J. Cryst. Growth **311**, 2033 (2009).
[31] N. Teraguchi, A. Suzuki, Y. Saito, T. Yamaguchi, T. Araki, and Y. Nanishi, J. Cryst. Growth **230**, 392 (2001).
[32] E. F. Schubert, *Design of Current Flow in Light Emitting Diodes* (Cambridge University Press, Cambridge, 2006), pp. 127–144.
[33] X. Xu, R. P. Vaudo, J. Flynn, and G. R. Brandes, J. Electron. Mater. **31**, 402 (2002).

Published under license by AIP Publishing